

Article

# Preparation and Adsorption Properties of Magnetic Molecularly Imprinted Polymers for Selective Recognition of 17 $\beta$ -Estradiol

Lanbo Bi, Jimin Shen, Zhuoran Yao, Jing Kang \*, Shengxin Zhao, Pengwei Yan, Binyuan Wang and Zhonglin Chen \*

State Key Laboratory of Urban Water Resources and Environment, School of Environment, Harbin Institute of Technology, Harbin 150090, China

\* Correspondence: jingkang@hit.edu.cn (J.K.); zhonglinchen@hit.edu.cn (Z.C.)

**Abstract:** In this paper, magnetic molecularly imprinted polymers (MMIPs) were fabricated on the surface of Fe<sub>3</sub>O<sub>4</sub> by surface molecular imprinting technology, which can selectively adsorb 17 $\beta$ -estradiol (E2). The optimized experiments demonstrated that MMIPs possessed the best adsorption capacity when methanol was used as the solvent and MAA was used as the crosslinking agent, with a molar ratio of E2: MMA: EGDMA as 1:4:50. SEM, FTIR, and XRD were employed to investigate the morphologies of MMIPs and the results demonstrated that the MMIPs that can selectively adsorb E2 were successfully prepared on Fe<sub>3</sub>O<sub>4</sub> particles. The adsorption experiments showed that 92.1% of E2 was adsorbed by the MMIPs, which is higher than the magnetic non-molecularly imprinted polymers (MNIPs). The Freundlich isotherm model was more suitable to describe the adsorption process of E2 by MMIPs. Meanwhile, MMIPs had a better recognition ability for E2 and its structural analogs such as estrone and estriol. The MMIPs still had good adsorption performance after methanol regeneration five times. The prepared MMIPs had the advantages of efficient adsorption ability and high reusability, so they can be applied for selective recognition and removal of E2.

**Keywords:** adsorption kinetics; Fe<sub>3</sub>O<sub>4</sub> particles; molecularly imprinted polymers; regeneration process; selective adsorption; 17 $\beta$ -estradiol



check for updates

**Citation:** Bi, L.; Shen, J.; Yao, Z.; Kang, J.; Zhao, S.; Yan, P.; Wang, B.; Chen, Z. Preparation and Adsorption Properties of Magnetic Molecularly Imprinted Polymers for Selective Recognition of 17 $\beta$ -Estradiol. *Separations* **2022**, *9*, 381. <https://doi.org/10.3390/separations9110381>

Academic Editor: Marco Pellegrini

Received: 2 November 2022

Accepted: 16 November 2022

Published: 21 November 2022

**Publisher's Note:** MDPI stays neutral with regard to jurisdictional claims in published maps and institutional affiliations.



**Copyright:** © 2022 by the authors. Licensee MDPI, Basel, Switzerland. This article is an open access article distributed under the terms and conditions of the Creative Commons Attribution (CC BY) license (<https://creativecommons.org/licenses/by/4.0/>).

## 1. Introduction

As their pollutants could simulate hormone actions required by organisms or act on the endocrine system, endocrine disruptor compounds (EDCs) have become an increasing concern in recent years [1]. According to a large number of previous reports, EDCs could not only lead to a reduction in sex hormone activity and secretion but could also cause irreversible damage to the nervous and immune systems of organisms and cause abnormal reproductive organs in various organisms [2,3]. 17 $\beta$ -estradiol (E2), as a natural estrogen, is often used in pharmaceutical production and animal husbandry [4], which might seriously damage the health of human beings and the ecosystem due to its stability, high carcinogenicity, and activity [5,6]. E2 was released into the environment through two main ways, E2 as a feed additive introduced through aquaculture wastewater [7] and the other through hospital wastewater in the urban drainage system, and then into the ecosystem [8]. According to ecotoxicology studies, the predicted no-effect concentration (PNEC) of E2 ranged from 1 to 5 ng/L [9,10]. Selective recognition of E2 is essential for high-sensitivity detection and removal of E2.

Adsorption is one of the most commonly used methods for E2 separation. Many existing adsorbents such as activated carbon and chitosan could effectively adsorb E2 [11]. Meanwhile, many novel adsorbents have been prepared to adsorb E2, such as biomass [12], biochar [13], graphene oxide [14], and chitosan composites [15]; however, these adsorbents were still unable to selectively adsorb E2 from complex samples.

Molecularly imprinted technology (MIT) can simulate the mutual recognition of antibodies and biological receptors, thus enabling the preparation of materials that recognize

the target based on shape, size, and functional groups [16]. In the molecularly imprinted process, template molecules and functional monomers are self-assembled by hydrogen bonding and electrostatic interaction, which then react with the cross-linking agent to form polymers [17]. The polymers are then washed with eluent to form holes with similar shapes and complementary functional groups to template molecules [18]. Due to the simplicity and selectivity of MIT, it has been successfully applied in chromatographic separation [19], drug identification [20], environmental detection [21], food analysis [22], and other fields.

Magnetic separation technology can rapidly separate magnetic particles from a solution by using magnets [23]. Many studies have reported that molecularly imprinted polymers were synthesized on magnetic particles by combining magnetic separation technology and MIT [24,25]. Magnetic molecularly imprinted polymers (MMIPs) not only have high efficiency and selective adsorption ability but also can be rapidly separated from the sample. Li et al. [26] synthesized magnetic molecularly imprinted polymers with atrazine as a template and  $\text{Fe}_3\text{O}_4$  as the carrier. The maximum binding amounts of the polymers were 1.89 mg/g. After five repeated uses, the binding ability of the polymers was not significantly decreased.

In this paper, MMIPs were fabricated using E2 as the template for the selective adsorption of E2 in water. Compared with traditional adsorbents, MMIPs can preferentially adsorb E2 among multiple pollutants, and thus provide efficient and directional removal of certain pollutants. The molar ratio of E2, MAA, and EDGMA was optimized to obtain the best-prepared conditions. SEM, XRD, and FTIR were carried out to analyze the mechanism of the MMIPs' synthesis process. The effects of various factors on the adsorption capacity of MMIPs for E2 were investigated and the adsorption process of MMIPs was investigated according to adsorption kinetics curves and adsorption isotherms. With estrone, estradiol, phenol, and sulfamethoxazole as competitive compounds, the adsorption selectivity of MMIPs for E2 was studied under single and multiple systems. The regeneration method of MMIPs was optimized and the reusability of the MMIPs was also evaluated.

## 2. Materials and Methods

### 2.1. Chemicals

E2, estriol (E3), EGDMA, estrone (E1), 3-(trimethoxysilyl)propyl methacrylate (MPS), 2,2'-azobis(2-isobutyronitrile) (AIBN), and sulfamethoxazole (SMX) were obtained from Aladdin Reagent Company (Shanghai, China).  $\text{FeCl}_3 \cdot 6\text{H}_2\text{O}$ , phenol, acetic acid, sodium acetate, ethylene glycol, and tetraethyl orthosilicate (TEOS) were supplied by Sinopharm Chemical Reagent Company (Shanghai, China). MAA, 4-vinyl pyridine, and acrylamide were purchased from Sigma-Aldrich (USA). AIBN was recrystallized in ethanol and preserved at 4 °C prior to use. Acetonitrile and methanol were HPLC-grade and purchased from Sigma-Aldrich (St. Louis, MO, USA). Milli-Q water purification system (Millipore, Bedford, MA, USA) was used to prepare ultrapure water.

### 2.2. Preparation of MMIPs

The preparation protocol and recognition mechanism of MMIPs are shown in Figure S1. Firstly, for the preparation of  $\text{Fe}_3\text{O}_4$  particles [27], 1.73 g of  $\text{FeCl}_3 \cdot 6\text{H}_2\text{O}$  was added into 35 mL ethylene glycol and thoroughly stirred to dissolve, then 3.83 g of anhydrous sodium acetate was added. The mixture was stirred continuously for 30 min and then transferred to 50 mL autoclave. The autoclave was heated to 200 °C for 8 h. After the reaction, the black precipitates were collected by a magnet. The prepared  $\text{Fe}_3\text{O}_4$  particles were washed with a large amount of ultrapure water and ethanol, respectively, and were dried at 60 °C for 12 h.

Secondly, for the preparation of  $\text{Fe}_3\text{O}_4 @ \text{SiO}_2 @ \text{MPS}$  [28], 100 mg of  $\text{Fe}_3\text{O}_4$  particles was weighed into a round bottom flask and 80 mL ethanol, 20 mL water, and 1.5 mL 30% ammonia water were added. After the reaction solution was fully stirred, 1 mL TEOS was added slowly and the reaction solution was stirred at 30 °C for 6 h. The prepared  $\text{Fe}_3\text{O}_4 @ \text{SiO}_2$  was collected with magnets and washed several times with ultrapure water and ethanol, then dried in vacuum at 60 °C. MPS with vinyl was used as the coupling

agent between  $\text{Fe}_3\text{O}_4@\text{SiO}_2$  and polymers. First, 100 mg of  $\text{Fe}_3\text{O}_4@\text{SiO}_2$  was weighed into a round bottom flask, then 95 mL ethanol, 5 mL water, and 5 mL MPS were added. The mixture was adjusted to pH 4 with acetic acid and stirred at 60 °C for 24 h. The products were collected by magnets and cleaned three times with ultrapure water and ethanol, then dried in vacuum at 60 °C.  $\text{Fe}_3\text{O}_4@\text{SiO}_2@\text{MPS}$  was obtained.

Finally, for the preparation of MMIPs [26], 0.15 mmol E2, and 0.6 mmol MAA were added in 24 mL acetonitrile and homogenized by ultrasonication for 5 min, then the mixture was stored in dark for 6 h. Next, 100 mg of  $\text{Fe}_3\text{O}_4@\text{SiO}_2@\text{MPS}$ , 7.5 mmol EGDMA, 50 mg AIBN, and 1 mL glycol as dispersing agent were added to the above solution. The reaction solution was mixed by ultrasonication for about 10 min, then filled with nitrogen for 20 min to remove oxygen. The reaction solution was heated to 60 °C under the protection of nitrogen and stirred mechanically for 12 h. The products were cleaned with the mixed solution of methanol and 1 mol/L sodium hydroxide solution (4:1, *v/v*) until E2 was detected by HPLC. The magnetic non-molecularly imprinted polymers (MNIPs) were synthesized in the same method as MMIPs without the addition of E2.

### 2.3. Characterization of MMIPs

The ultraviolet absorption spectrum of the mixed solution was performed by UV-visible spectrophotometer (Beijing Purkinje General Company, Beijing, China). The morphologies of MMIPs and MNIPs were characterized by Scanning Electron Microscope (ZEISS, Oberkochen, Germany). X-ray Diffractometer (Panalytical B.v, Almelo, The Netherlands) and Fourier Transform Infrared Spectroscopy (PerkinElmer, Waltham, MA, USA) were used for characterization of the functional groups and crystal structures of MMIPs.

### 2.4. HPLC Analysis

An Agilent 1200 series HPLC system, equipped with a quaternary pump, an autosampler, a column compartment, a vacuum degasser, and an ultraviolet detector was used for the determination of E2, E1, E3, BPA, SMX, and phenol. The detection wavelength was 205 nm. The chromatographic column was a 250 mm × 4.6 mm, 5 μm ZORBAX SB-C18 column (Agilent, Santa Clara, CA, USA). The best mobile phase was acetonitrile and water (44:56, *v/v*) and the flow rate was 1.0 mL/min with an injection volume of 100 μL.

### 2.5. Adsorption Experiments

The adsorption kinetics of MMIPs was performed by suspending 10 mg of MMIPs in the 20 mL of 5 mg/L E2 solution in a conical flask, with the sample solution oscillated at 25 °C air bath. The supernatant was filtered with a 0.22 μm membrane and HPLC was used to determine the remaining concentration of E2 in the supernatant after adsorption at different times. In the isothermal adsorption experiment, the adsorption capacities of MMIPs for E2 with different concentrations (0.5–10 mg/L) were studied by the above method, except that the sample was shaken for 12 h to reach adsorption equilibrium. The adsorption amount of MMIPs (*Q*, mg/g) and removal efficiency were obtained following Equations (S1) and (S2) in Supplementary Materials [29]. The isotherm models used in the research are displayed in Equations (S5) and (S6) in Supplementary Materials [30].

The distribution coefficient (*K*) usually represented the binding ability of the adsorbent for the compound and the *K* was calculated as the following equation:

$$K = C_p / C_e, \quad (1)$$

$$C_p = (C_0 - C_e), \quad (2)$$

where  $C_p$  is the concentration of E2 adsorbed on the polymers, and  $C_0$  and  $C_e$  are the initial and equilibrium concentrations of E2 in the sample. The imprinting factor (IF) and selection factor ( $\alpha$ ) were used to represent the ability of MMIPs to recognize other

competing molecules. The correlation adsorption parameters were calculated according to the following equations [31]:

$$IF = K_{MMIPs}/K_{MNIPs}, \quad (3)$$

$$\alpha = IF_1/IF_2, \quad (4)$$

where  $K_{MMIPs}$  and  $K_{MNIPs}$  are the distribution coefficients of MMIPs and MNIPs, respectively.  $IF_1$  and  $IF_2$  represent the imprinting factors of competitive molecules and E2, respectively.

The process of regeneration and reusability of MMIPs is listed in Supplementary Materials.

### 3. Results and Discussion

#### 3.1. Optimization of MMIPs Preparation Conditions

Various factors could influence the adsorption capacity, such as the type of solvent and the ratio of synthetic sources. The organic solvent was used to prepare the MMIPs because the template and functional monomer were bonded by hydrogen bonding [32]. Methanol, ethanol, acetonitrile, tetrahydrofuran, and dichloromethane were used to evaluate the influence of reaction solvents on the adsorption capacity of MMIPs. Meanwhile, the functional monomers' effect on the adsorption performance of MMIPs was assessed by using MAA, acrylamide, and 4-vinyl pyridine, as displayed in Figure S2a,b. When MAA was used as the functional monomer and acetonitrile as the solvent, the adsorption performance of MMIPs was the best. In addition, the effects of the molar ratio of template to functional monomer (E2: MAA), of 1:2, 1:4, 1:6, 1:8, and 1:10, on the adsorption performance of MMIPs were studied. Meanwhile, the optimum ratio of template to cross-linker (E2: EGDMA) was also tested. The experimental results are shown in Figure S2c,d, indicating that the optimum synthesis molar ratio of E2: MMA: EGDMA was 1:4:50.

In this experiment, the ultraviolet absorption curves of E2, MAA, and the mixture of E2 and MAA in acetonitrile solution were investigated to study the hydrogen bonding between the template and functional monomer. As shown in Figure 1, when MAA was added to the E2 solution, the mixed solution's maximum absorption wavelength in the spectrum was redshifted, indicating that hydrogen bonding between E2 and MAA was generated. Moreover, the absorbance of the mixed solution was significantly higher than the sum of E2 and MAA's absorbance at the maximum absorption peak, which also indicated the presence of hydrogen bonding between E2 and MAA.

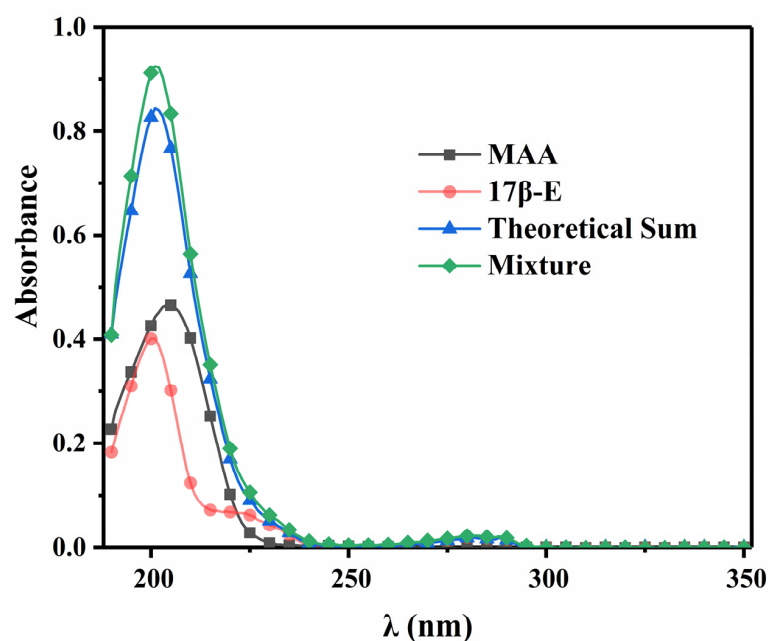


Figure 1. Ultraviolet absorption spectra of E2, MAA, and mixture of E2 and MAA in acetonitrile solution.

### 3.2. Characterization of MMIPs

The SEM images of Fe<sub>3</sub>O<sub>4</sub> particles and MMIPs are presented in Figure 2a,b. Fe<sub>3</sub>O<sub>4</sub> particles were regular spheres with a diameter of about 70–300 nm. Because of the small diameter, Fe<sub>3</sub>O<sub>4</sub> could be easily assembled by polymerization. The SEM images of MMIPs displayed the polymer coating on the surface of Fe<sub>3</sub>O<sub>4</sub>, which would provide higher specific surface areas and enhance the sorption capacity of MMIPs.

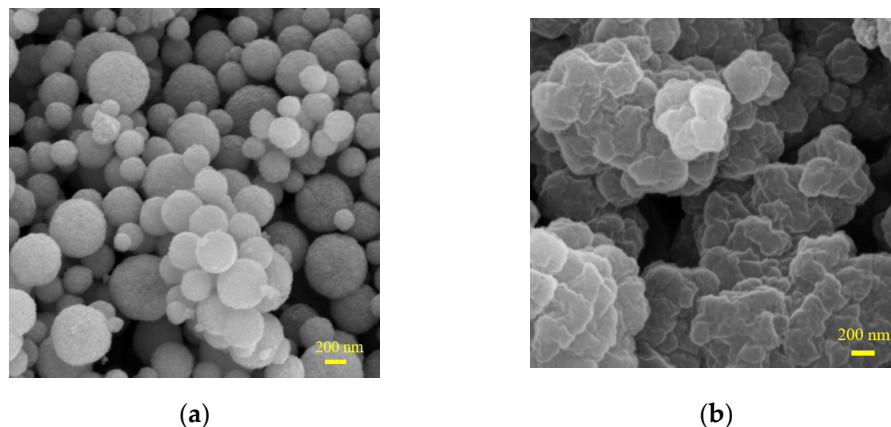


Figure 2. SEM images of (a) Fe<sub>3</sub>O<sub>4</sub> and (b) MMIPs.

The FTIR spectra of Fe<sub>3</sub>O<sub>4</sub>, Fe<sub>3</sub>O<sub>4</sub>@SiO<sub>2</sub>@MPS, and MMIPs are presented in Figure 3a. The signal at 587 cm<sup>-1</sup> belongs to an Fe-O bond, indicating that Fe<sub>3</sub>O<sub>4</sub> was prepared by the solvothermal method. Compared with Fe<sub>3</sub>O<sub>4</sub>, the peaks of Fe<sub>3</sub>O<sub>4</sub>@SiO<sub>2</sub>@MPS at 800 and 1100 cm<sup>-1</sup> were related to the vibration of Si-O-Si and Si-O bonds, respectively, indicating that SiO<sub>2</sub> was coated on the surface of Fe<sub>3</sub>O<sub>4</sub>. The absorption peaks of the C=O bond at 1730 cm<sup>-1</sup> and the C-H bond at 2917 cm<sup>-1</sup> were derived from the MPS in the FTIR spectrum of Fe<sub>3</sub>O<sub>4</sub>@SiO<sub>2</sub>@MPS, suggesting that Fe<sub>3</sub>O<sub>4</sub>@SiO<sub>2</sub>@MPS was successfully prepared. Compared with Fe<sub>3</sub>O<sub>4</sub>@SiO<sub>2</sub>@MPS, the characteristic band of C=O at 1730 cm<sup>-1</sup> of MMIPs was stronger, indicating successful polymerization.

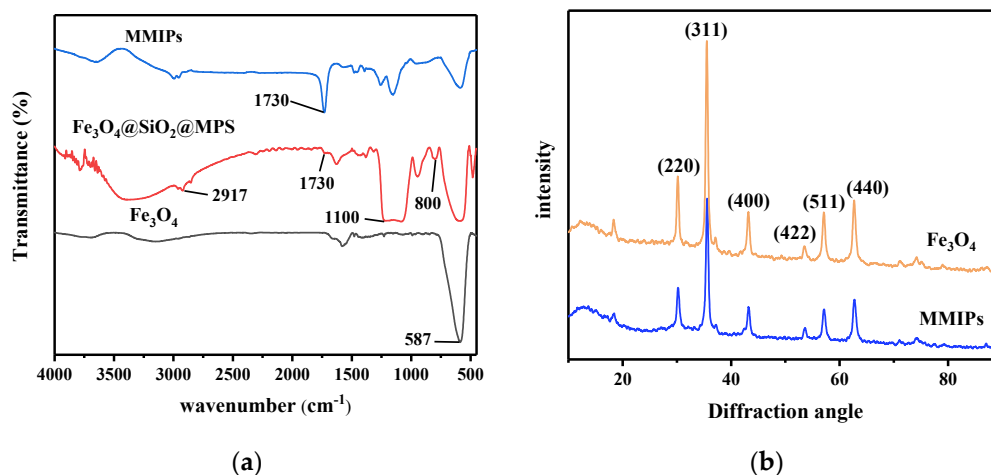


Figure 3. (a) FTIR spectra of Fe<sub>3</sub>O<sub>4</sub>, Fe<sub>3</sub>O<sub>4</sub>@SiO<sub>2</sub>@MPS, and MMIPs; (b) XRD patterns of Fe<sub>3</sub>O<sub>4</sub> and MMIPs.

The crystal phases of Fe<sub>3</sub>O<sub>4</sub> and MMIPs were analyzed by XRD in Figure 3b. In the 2θ region of 10–90°, the six diffraction peaks appeared in both Fe<sub>3</sub>O<sub>4</sub> and MMIPs at angles 30.02°, 35.48°, 43.28°, 53.55°, 57.05°, and 62.68°, which match with the crystallographic plane of Fe<sub>3</sub>O<sub>4</sub> (220, 311, 400, 422, 511, and 440) according to JCPDS (JCPDS No. 19-629). The presence of diffraction peaks in the XRD patterns indicated that the phase component

was not changed during the preparation process. The nitrogen adsorption–desorption isotherm of MMIPs, a typical IV isotherm with an H3 hysteresis loop, is displayed in Figure 4. The BET-specific surface area and total pore volume of MMIPs were  $4.1618 \text{ m}^2/\text{g}$  and  $0.032025 \text{ cm}^3/\text{g}$ , respectively.

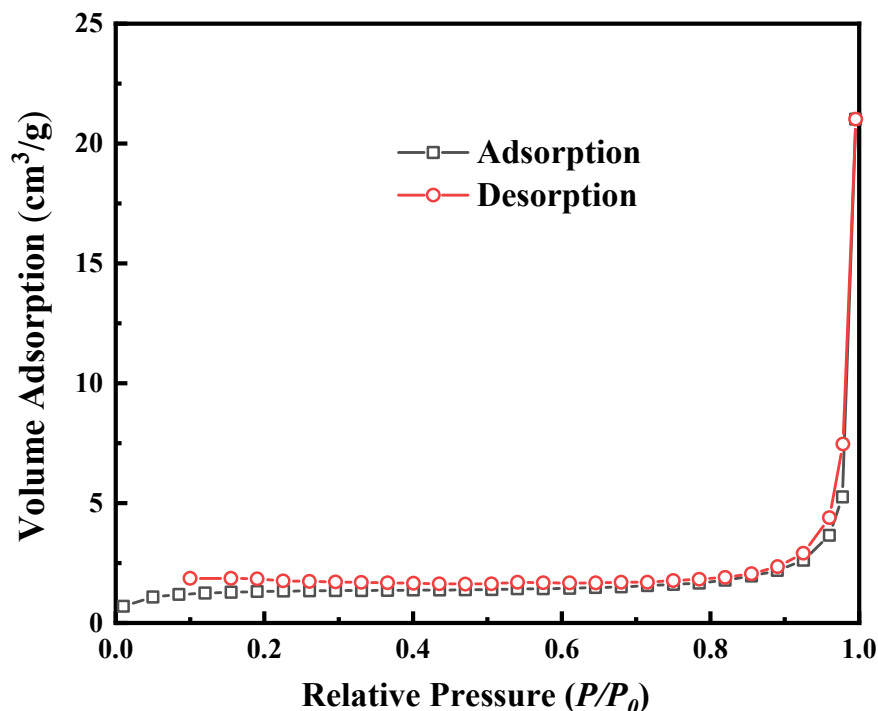


Figure 4. Nitrogen adsorption–desorption isotherm of MMIPs.

### 3.3. Adsorption Performance

#### 3.3.1. Adsorption Kinetics

The adsorption kinetics curves of E2 by MMIPs and MNIPs were investigated in this study. From Figure 5, the adsorption rates of MMIPs and MNIPs were fast in the first 5 min and the adsorption equilibrium was reached when the experiment was performed for about 40 min. The results showed that the adsorption process of MMIPs for E2 was first fast and then slow. In the initial stage of the reaction, the adsorption site on the surface of MMIPs adsorbed E2 to reduce the binding energy. At this time, the adsorption occurred on the surface of the polymers and the rate was very fast. Then the adsorption occurred inside the MMIPs, which slowed the rate.

For further study, the pseudo-first-order and pseudo-second-order kinetics models were selected to analyze the kinetics process of MMIPs for E2; the fitting parameters of the models were also adopted to investigate the kinetic process of MMIPs. Table S1 shows the fitting equations and correlation parameters of the two kinetic models. There was a good linear relationship between both kinetic models because their correlation coefficient was close to 1 and the sum of square of errors (SSE) was employed to evaluate the suitability of the model [33]. The SSE of the pseudo-second-order kinetics model (0.1219) was lower than that of the pseudo-first-order kinetics model (0.7444), suggesting that the latter one was more appropriate for the sorption reaction of E2 by MMIPs. The adsorption rate was controlled by the chemical adsorption mechanism and the unoccupied adsorption sites on MMIPs positively affected the rate of the adsorption process [34].

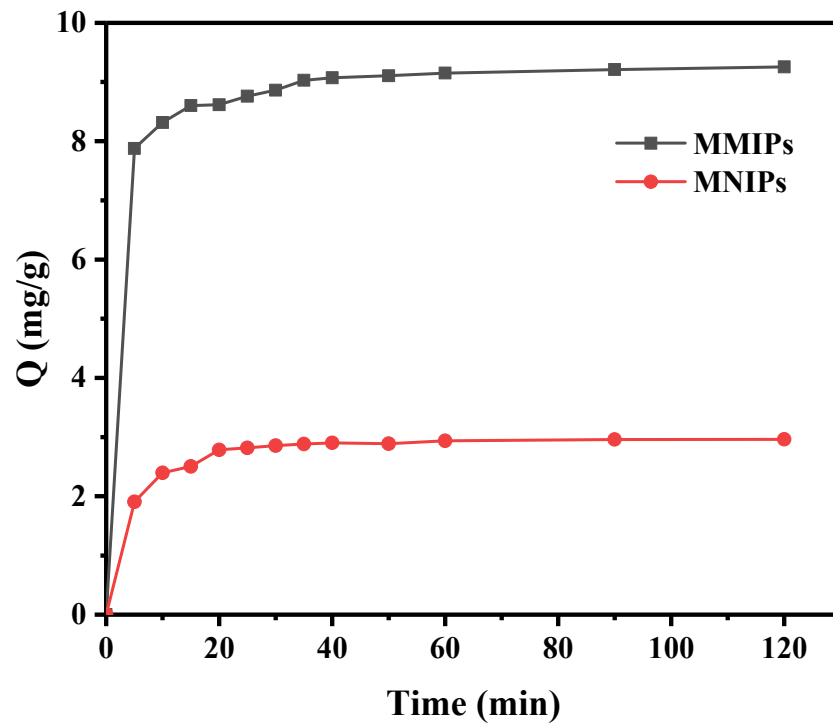


**Figure 5.** Adsorption kinetic curves of MMIPs and MNIPs. Conditions:  $[E2]_0 = 5 \text{ mg/L}$ ,  $[MMIPs \text{ or } MNIPs]_0 = 0.5 \text{ g/L}$ ,  $T = 30 \text{ }^\circ\text{C}$ , and  $\text{pH} = 6.0$ .

### 3.3.2. Adsorption Isotherms

The adsorption amounts of MMIPs and MNIPs at different initial E2 concentrations are presented in Figure 6a. The adsorption amounts of both adsorbents were positively correlated with the E2 concentration of the sample solution. The adsorption amounts of MNIPs increased slowly when the initial E2 concentration of the sample solution was higher than 8 mg/L. Additionally, the adsorption amounts of the MMIPs were always bigger than that of MNIPs.

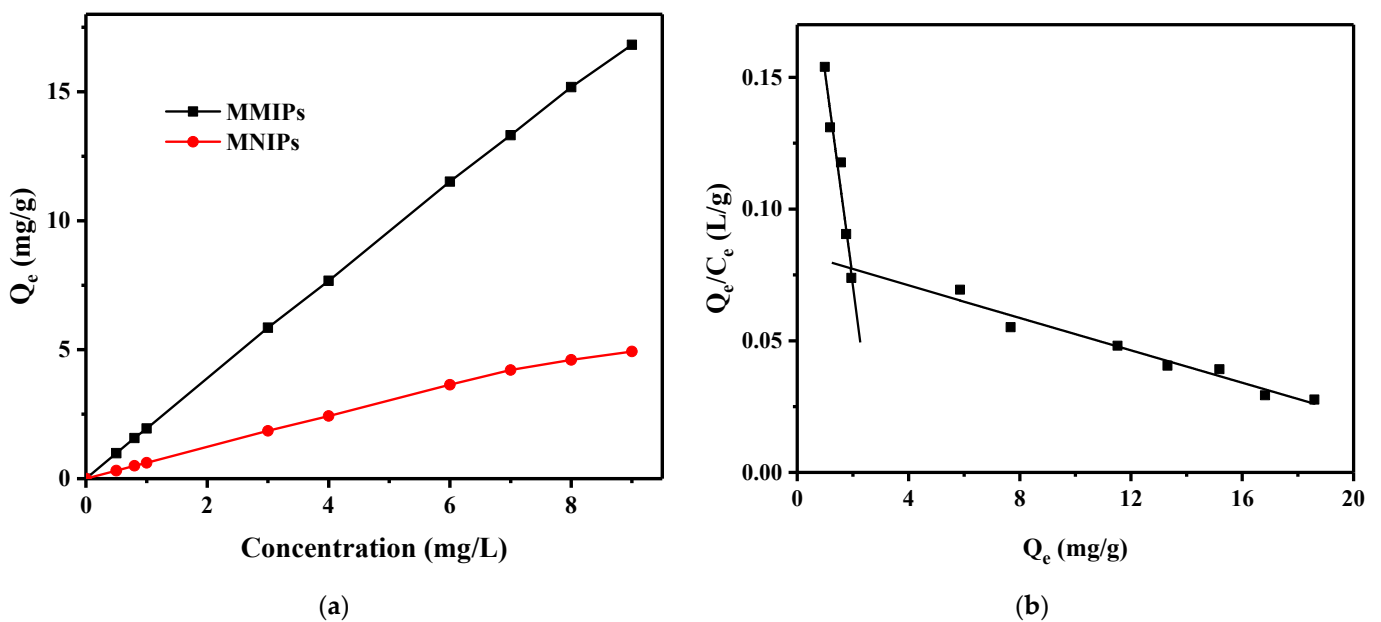


**Figure 6.** (a) Adsorption isotherms of MMIPs and MNIPs, and (b) Scatchard curve of MMIPs. Conditions:  $[E2]_0 = 5 \text{ mg/L}$ ,  $[MMIPs \text{ or } MNIPs]_0 = 0.5 \text{ g/L}$ ,  $T = 30 \text{ }^\circ\text{C}$ , and  $\text{pH} = 6.0$ .

The Langmuir isotherm model describes the single-layer adsorption process and the Freundlich isotherm model describes the multi-layer adsorption process [35]; these two models are often adopted to investigate the isothermal adsorption of MMIPs. The Langmuir and Freundlich adsorption isotherm equations were selected to fit the adsorption amounts of MMIPs and MNIPs by reaching the adsorption equilibrium at various initial E2 concentrations, respectively. Table S2 showed the model fitting parameters and the SSE of the Freundlich isotherm equation of MMIPs and MNIPs ( $SSE_{MMIPs} = 3.381$  and  $SSE_{MNIPs} = 0.2127$ ) were both weaker than that of the Langmuir isotherm equation ( $SSE_{MMIPs} = 5.4920$  and  $SSE_{MNIPs} = 0.4351$ ). Therefore, compared with the Langmuir adsorption isotherm equation, the Freundlich adsorption isotherm equation was more suitable to analyze the adsorption behavior of MMIPs for E2, which indicated the adsorption behavior of MMIPs for E2 was multi-layer adsorption and the adsorption sites on MMIPs were not uniformly distributed [36].

The saturated binding concentration of MMIPs and the types of MMIPs binding sites were studied by the Scatchard model [37]. The relationship between  $Q_e/C_e$  and  $Q_e$  based on the Scatchard model is shown in Figure 6b. The fitting curves showed two different linear relationships in different ranges, indicating there were high-affinity and low-affinity adsorption sites on MMIPs. The Scatchard parameters of the fitting curves were shown in Table S3.

### 3.3.3. Adsorption Selectivity

E3 and E1, as structural analogs of E2, and SMX and phenol, as coexisting competitors of E2, were employed to investigate the selectivity adsorption of MMIPs for E2 in a single system and multiple system. The molecular structures of the five compounds are shown in Figure S3. As shown in Figure 7a, MMIPs had the largest adsorption amount for E2 due to their selective adsorption sites. The binding capacity of MMIPs to E1 and E3 was slightly weaker than that of E2 because of the similar molecular structures to E2. For coexisting competitors (SMX and phenol), the binding capacity of MMIPs was significantly reduced.

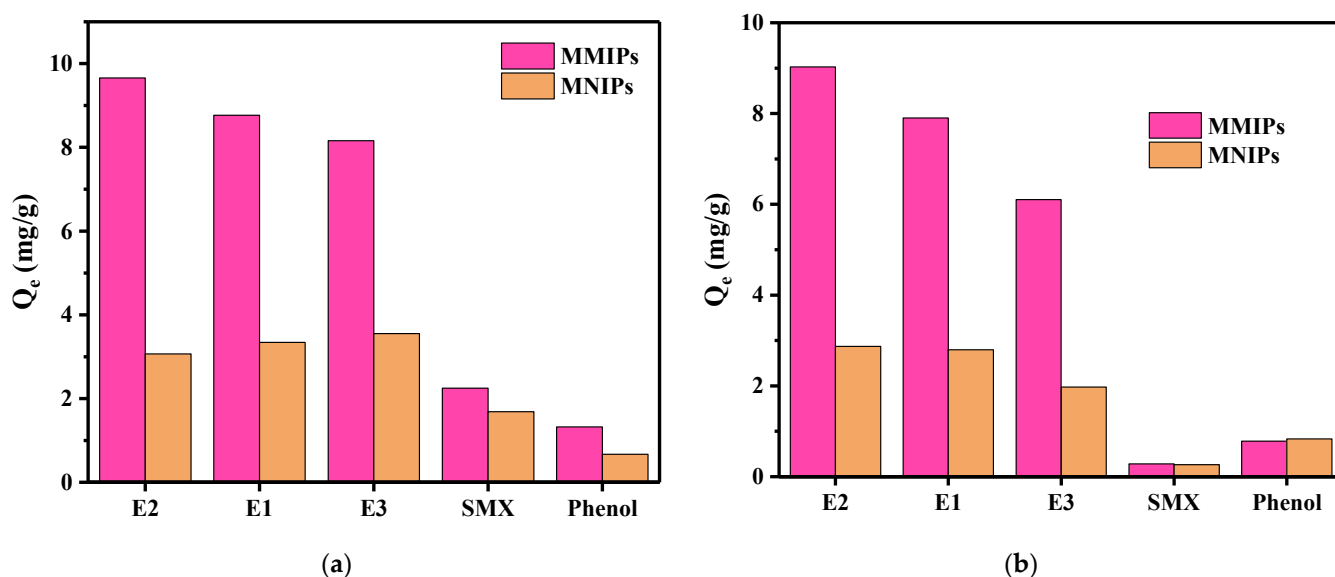


**Figure 7.** Adsorption capacity of MMIPs and MNIPs for E2 and other four compounds in: (a) single system, and (b) multiple system. Conditions:  $[E2 \text{ or other compounds}]_0 = 5 \text{ mg/L}$ ,  $[MMIPs \text{ or MNIPs}]_0 = 0.5 \text{ g/L}$ ,  $T = 30 \text{ }^\circ\text{C}$ , and  $\text{pH} = 6.0$ .

Compared with the molecular structure of E2, there was an OH group replaced by a carbonyl group in E1 and the loss of an OH group in E3, which led to a decrease in the binding capacity of the MMIPs. Phenol has an OH group on the benzene ring that could form hydrogen bonds with MMIPs but its molecular structure was much smaller

than that of E2, leading to the lower adsorption selectivity. Due to the molecular structure and functional groups of SMX being different from E2, MMIPs showed relatively lower adsorption capability and weaker selectivity to SMX. Above all, the selective recognition ability of MMIPs depends on the functional groups, size, and shape of the compounds [38].

The adsorption performance of MMIPs for each compound in a multiple-system solution decreased compared with that of the single system in Figure 7b. However, the adsorption amounts of MMIPs for E2, E1, and E3 were higher than that for phenol and SMX. Three parameters ( $K$ , IF, and  $\alpha$ ) were also used to evaluate the selective recognition ability of MMIPs [39]. The values of the three parameters are shown in Table 1.  $K$  represents the binding performance of MMIPs and MNIPs to the compound, and the value of  $K$  was positively correlated with the adsorption capacity of the adsorbent to the compound. Meanwhile, IF represents the selective recognition ability of MMIPs for analytes, and the highest IF value of E2 indicated that MMIPs could selectively recognize E2.

**Table 1.** Selectivity coefficient data of MMIPs and MNIPs for E2 and other four compounds.

Analytes	$K_{\text{MMIPs}}$	$K_{\text{MNIPs}}$	IF	$\alpha$
E2	28.32	0.44	64.02	
E1	7.11	0.50	14.14	4.53
E3	4.43	0.55	8.04	7.96
SMX	0.29	0.20	1.43	44.76
Phenol	0.15	0.07	2.13	29.99

### 3.4. Effects of Parameters on Adsorption Performance

The adsorption amounts of MMIPs can be easily affected by the reaction circumstances during the adsorption process. The variation in adsorption performance under different adsorption conditions could further explain the adsorption mechanism. The temperature and pH of the adsorption solution were investigated for their effects on the adsorption capacity of E2 by MMIPs.

The effects of temperatures between 15 °C and 35 °C on the adsorption process were evaluated and the results are shown in Figure 8a. When the temperature increased from 15 °C to 30 °C, the adsorption amounts of MMIPs were improved and, subsequently, the increase in temperature had little effect on the adsorption capacity. Therefore, the mass transfer rate between adsorbent and pollutants is positively correlated with temperature, and with the increase in adsorption temperature, the adsorption rate also increases.

Importantly, pH conditions can affect both the present form of E2 in the solution and the surface charge of the adsorbent [40]. The effects of a pH between four and eight on the adsorption of E2 by MMIPs were evaluated. As shown in Figure 8, when pH was in the range of 4~6, the binding capacity of MMIPs for E2 was positively correlated with the pH conditions; however, when pH > 6, the binding capacity of MMIPs was negatively correlated with the sample solution of pH. This may be due to the fact that the zero charge point of MMIPs (5.45, as implied in Figure S4) and the surface charge of MMIPs changes from positive to negative when pH > 6. According to previous reports [41], when the adsorption solution was in a neutral state, the interactions between the adsorbent and pollutants mainly occurred through Van der Waals forces and hydrogen bonding. However, when the solution was alkaline, the carboxylic acid group on the MMIPs and the hydroxyl group on estradiol would dissociate, which reduced the adsorption performance. The dissociation constant ( $pK_a$ ) of E2 is 10.72, when pH > 7, E2 exists in the mixture of anion and molecular form. The hydroxyl group in E2 molecule will lose  $H^+$  ions because of ionization in alkaline media and hinder the H-bond forming accordingly, which leads to the reduction in the adsorption capacity of MMIPs under alkaline conditions [42].

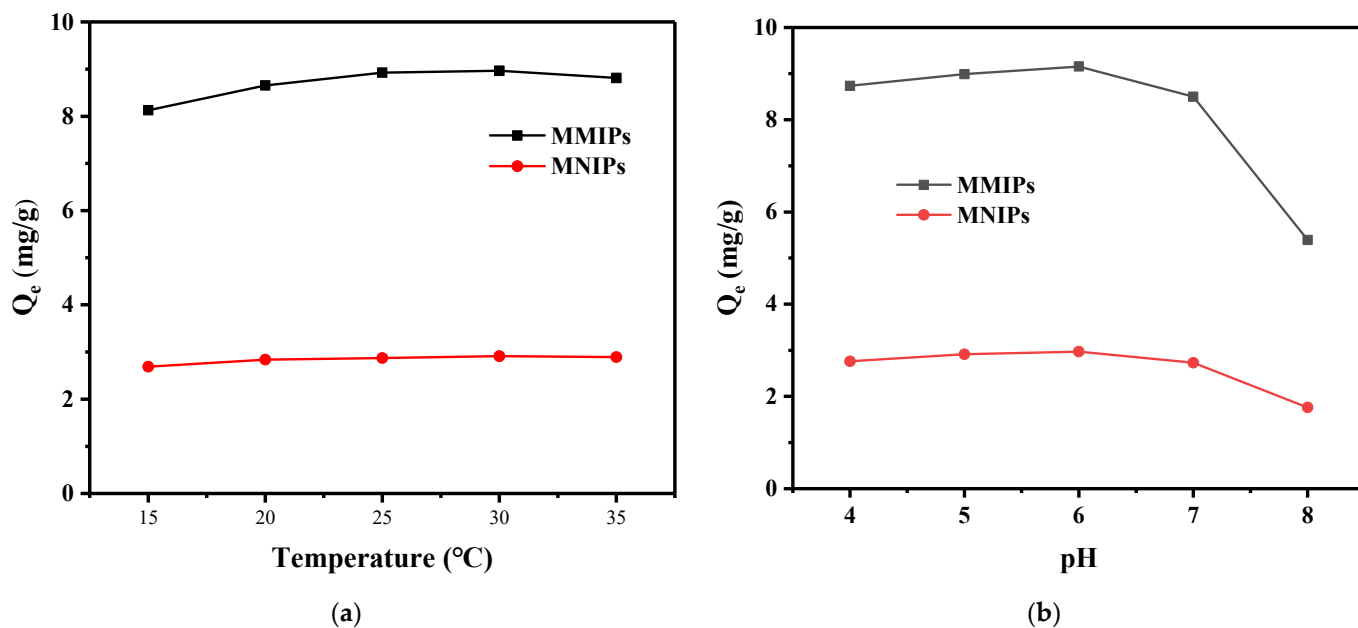


**Figure 8.** The effects of (a) temperature and (b) pH on adsorption process. Conditions:  $[E2]_0 = 5 \text{ mg/L}$ ,  $[MMIPs \text{ or } MNIPs]_0 = 0.5 \text{ g/L}$ ,  $T = 30 \text{ }^\circ\text{C}$ , and  $\text{pH} = 6.0$ .

The effect of the MMIP’s dosage on the removal efficiency for E2 was investigated at three levels (0.25, 0.5, and 1.0 g/L). As displayed in Figure 9a, the removal of E2 improved with the enhancement of MMIPs dosage. Compared with the adsorbent dosage of 0.5 g/L, the removal of E2 was not significantly improved at 1.0 g/L of MMIPs, indicating that the adsorption sites in the reaction solution reached saturation. The influence of the substrates in the actual water for E2 removal efficiency was investigated based on the adsorption performance of MMIPs in tap water and source water, as displayed in Figure 9b. Compared with ultrapure water, the removal efficiency of E2 in tap water and source water decreased slightly but the reduction was not obvious, indicating that MMIPs could preferentially adsorb E2 in the presence of exogenous ions and natural organic pH matter.

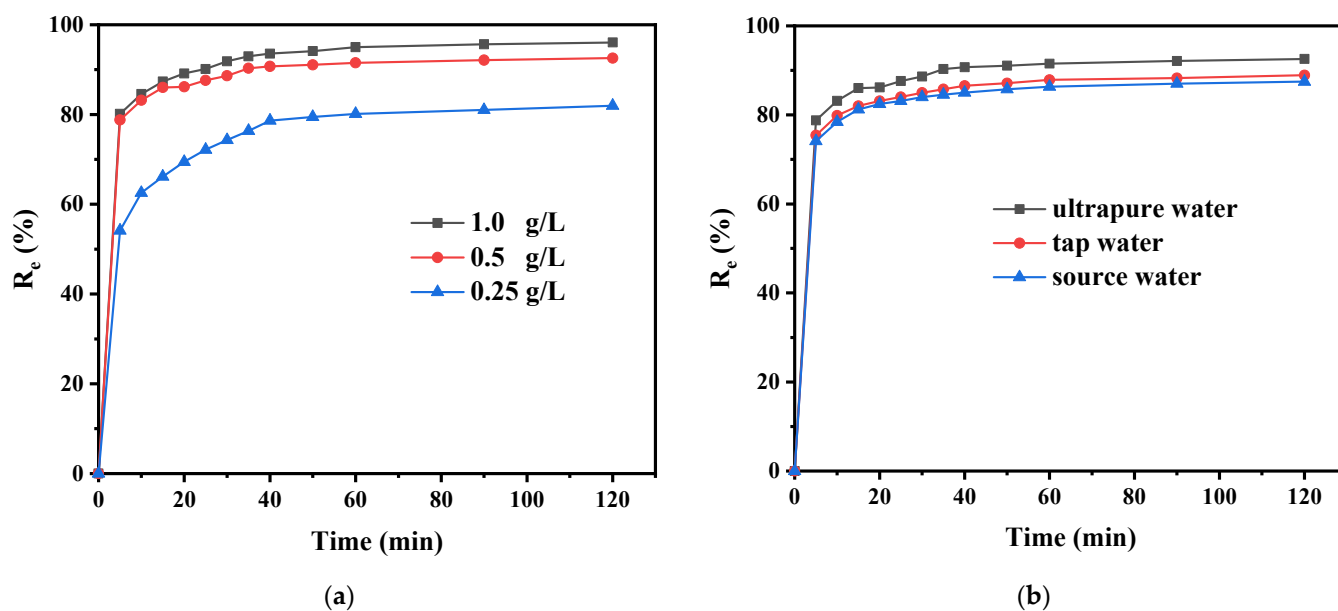


**Figure 9.** (a) The effect of MMIPs dosage on the removal efficiency for E2. (b) Removal efficiency of E2 by MMIPs in different water bodies. Conditions:  $[E2]_0 = 5 \text{ mg/L}$ ,  $[MMIPs \text{ or } MNIPs]_0 = 0.5 \text{ g/L}$ ,  $T = 30 \text{ }^\circ\text{C}$ , and  $\text{pH} = 6.0$ .

### 3.5. Possible Mechanism

According to the above analysis, the preparation and recognition mechanism of MMIPs for E2 are displayed in Figure S1. Firstly, E2 and MAA formed the precursor through hydrogen bonding during the preparation process, which was polymerized into MMIPs after the preparation reaction. Subsequently, E2 in MMIPs was eluted by elution agents, producing the adsorption site for E2 in MMIPs. When MMIPs were added to the water contaminated by E2, the specific active sites would preferentially adsorb E2 and were not interfered with by other pollutants, thus achieving the priority removal of E2 in the water.

### 3.6. Regeneration and Reusability of MMIPs

The regeneration and reuse of adsorbent were also important indexes to evaluate its performance. In the experiment, the four regenerative solvents, methanol, ethanol, acetone, and acetonitrile, were used to investigate the regeneration of adsorption-saturated MMIPs and the effects of regenerative time and frequencies on regeneration efficiency were also investigated. As shown in Figure 10a, the best regenerative solvent for MMIPs was methanol, so methanol would be used for regeneration when MMIPs reached adsorption saturation.

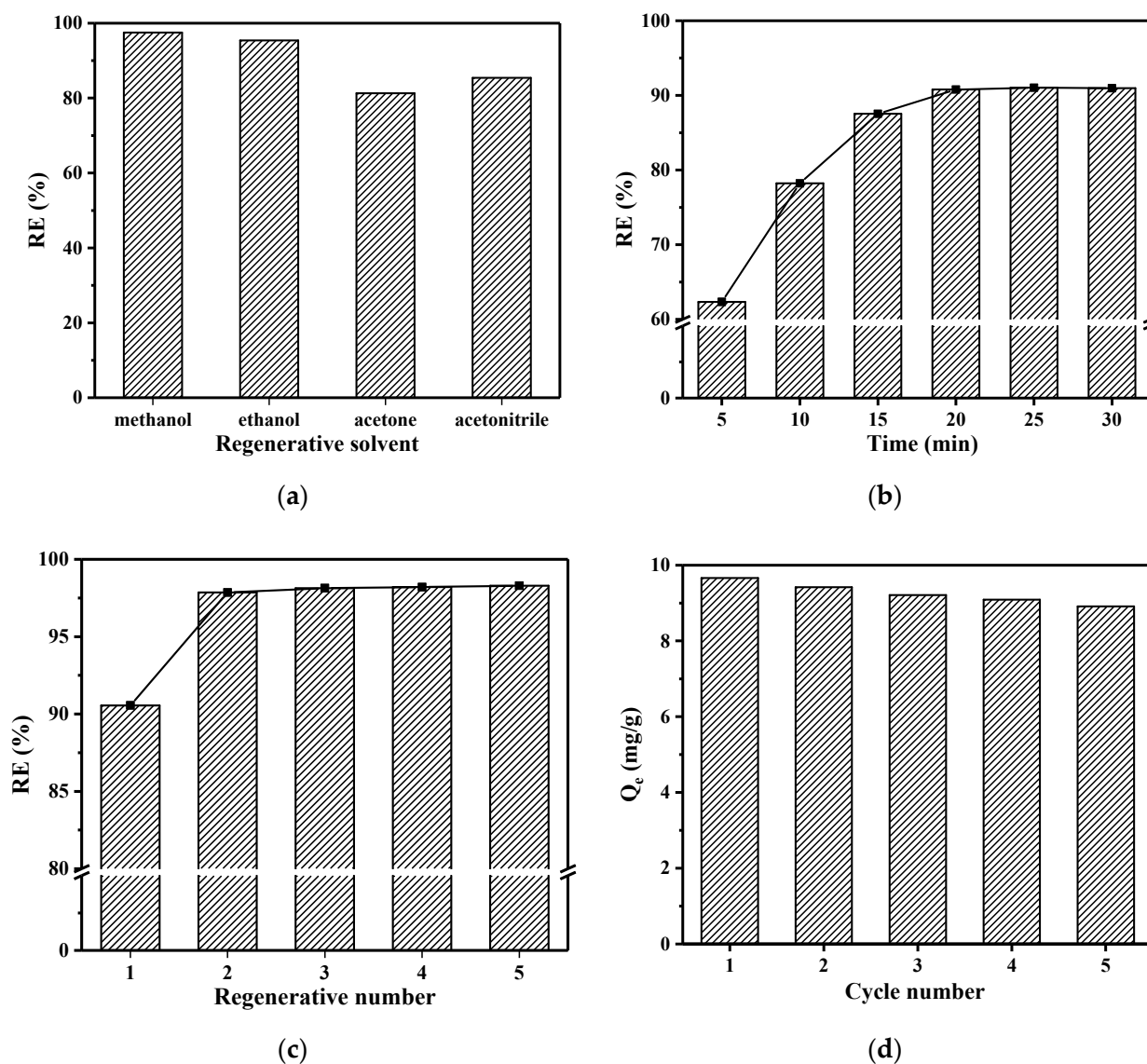


**Figure 10.** The effects of: (a) regenerative solvents, (b) regeneration time, and (c) regeneration number on regeneration of MMIPs. (d) Reusability of MMIPs on adsorption of E2. Conditions:  $[E2]_0 = 5 \text{ mg/L}$ ,  $[MMIPs \text{ or } MNIPs]_0 = 0.5 \text{ g/L}$ ,  $T = 30 \text{ }^\circ\text{C}$ , and  $\text{pH} = 6.0$ .

The experiment on the effect of regeneration time was carried out by suspending the adsorbed saturated MMIPs in the methanol and oscillating for 5–30 min in an oscillating chamber at 25 °C. The regeneration efficiencies of MMIPs are shown in Figure 10b, which were positively correlated with regeneration time in the first 20 min and the regeneration efficiency remained unchanged after 20 min, so the regeneration time was selected as 20 min. The influence of regeneration frequencies (1–5) on regeneration efficiency was investigated. As shown in Figure 10c, after two times of regeneration, the regeneration efficiency reached 98% and subsequent regeneration did not improve efficiency much. Therefore, the adsorption-saturated MMIPs were regenerated two times, and the regeneration conditions were 10 mL methanol as the regeneration solvent and 20 min of regeneration time.

The reusability of MMIPs was performed by investigating the adsorption capacity of MMIPs under different cycle times when methanol was used as the regenerative solvent. Figure 10d displays that the binding ability of MMIPs for E2 hardly decreased after at least five times of reuse.

#### 4. Conclusions

In this work, MMIPs were prepared by MIT and magnetic separation techniques for the adsorption of natural estrogen E2. Firstly, MMIPs with the maximum adsorption capacity were obtained by optimizing their preparation conditions. SEM, FTIR, and XRD were employed to demonstrate the surface structure and morphology of MMIPs; the results indicated that polymers were successfully synthesized on Fe<sub>3</sub>O<sub>4</sub>. The adsorption experiments indicated that MMIPs had larger adsorption amounts and a faster adsorption rate for E2 than MNIPs, which was attributed to the existence of both high-affinity binding sites and low-affinity binding sites on MMIPs. The selective adsorption experiment also showed that compared with MNIPs, MMIPs not only had a larger adsorption capacity for E2 but also had better adsorption capacity for analogs of E2. Finally, the optimal regeneration method of adsorbed saturated MMIPs was studied. The purpose of this paper was to develop an effective adsorbent for the selective recognition and removal of E2.

**Supplementary Materials:** The following supporting information can be downloaded at: <https://www.mdpi.com/article/10.3390/separations9110381/s1>, Table S1: Kinetic parameters for the adsorption of E2 on MMIPs; Table S2: Adsorption isotherm constants for adsorption of E2 on MMIPs; Table S3: Scatchard parameters for the adsorption of E2 on MMIPs; Table S4: Adsorption performance of E2 by other adsorbents [43–51]. Figure S1: Schematics of synthesis and recognition E2 of MMIPs; Figure S2: Effect of synthetic conditions on the adsorption ability of MMIPs for E2: (a) reaction solvent, (b) functional monomer, and (c) molar ratio of E2: MAA, (d) molar ratio of E2: EDGMA; Figure S3: The molecular structures of (a) E2, (b) E1, (c) E3, (d) SMX, and (e) phenol. Figure S4: Zeta potential value of MMIPs at different pH.

**Author Contributions:** L.B.: Conceptualization, Methodology, Formal analysis, Investigation, and Writing—original draft. J.S.: Project administration. Z.Y.: Investigation. J.K.: Funding acquisition, Writing—review and editing. S.Z.: Supervision. P.Y.: Resources. B.W.: Supervision. Z.C.: Funding acquisition, Resources, and Project administration. All authors have read and agreed to the published version of the manuscript.

**Funding:** This work was supported by the National Key R&D Program of China (Grant No. 2019YFD1100104), the National Natural Science Foundation of China (Grant No. 51608148), the State Key Laboratory of Urban Water Resources and Environment (Harbin Institute of Technology) (Grant No. 2021TS16), and the Heilongjiang Touyan Innovation Team Program (Grant No. HIT-SE-01).

**Institutional Review Board Statement:** Not applicable.

**Data Availability Statement:** The data are included as Supplementary Materials. However, the raw data will be available upon request.

**Acknowledgments:** The authors wish to acknowledge the experimental space and equipment from Harbin Institute of Technology, School of the Environment, and the State Key Laboratory of Urban Water Resources and Environment.

**Conflicts of Interest:** The authors declare no conflict of interest.

## References

1. Sutherland, D.L.; Ralph, P.J. Microalgal bioremediation of emerging contaminants—Opportunities and challenges. *Water Res.* **2019**, *164*, 114921. [[CrossRef](#)] [[PubMed](#)]
2. Adeel, M.; Song, X.; Wang, Y.; Francis, D.; Yang, Y. Environmental impact of estrogens on human, animal and plant life: A critical review. *Environ. Int.* **2017**, *99*, 107–119. [[CrossRef](#)] [[PubMed](#)]
3. Nie, M.H.; Yang, Y.; Liu, M.; Yan, C.X.; Shi, H.; Dong, W.B.; Zhou, J.L. Environmental estrogens in a drinking water reservoir area in Shanghai: Occurrence, colloidal contribution and risk assessment. *Sci. Total Environ.* **2014**, *487*, 785–791. [[CrossRef](#)] [[PubMed](#)]
4. Adeel, M.; Zain, M.; Fahad, S.; Rizwan, M.; Ameen, A.; Yi, H.; Baluch, M.A.; Lee, J.Y.; Rui, Y.K. Natural and synthetic estrogens in leafy vegetable and their risk associated to human health. *Environ. Sci. Pollut. Res.* **2018**, *25*, 36712–36723. [[CrossRef](#)] [[PubMed](#)]
5. Bilal, M.; Iqbal, H.M.N. Persistence and impact of steroidal estrogens on the environment and their laccase-assisted removal. *Sci. Total Environ.* **2019**, *690*, 447–459. [[CrossRef](#)] [[PubMed](#)]
6. Hu, S.Q.; Zhang, H.C.; Shen, G.X.; Yuan, Z.J.; Xu, T.; Ji, R. Effects of 17 beta-estradiol and 17 alpha-ethinylestradiol on the embryonic development of the clearhead icefish (*Protosalanx hyalocranius*). *Chemosphere* **2017**, *176*, 18–24. [[CrossRef](#)]
7. Diaz-Quiroz, C.; Gonzalez, L.; Alvarez, M.S.; Hernandez-Chavez, J.F.; Rodriguez, A.; Deive, F.J.; Ulloa-Mercado, G. Biocompatible amino acid-based ionic liquids for extracting hormones and antibiotics from swine effluents. *Sep. Purif. Technol.* **2020**, *250*, 117068. [[CrossRef](#)]
8. Ana, K.M.S.; Espino, M.P. Occurrence and distribution of hormones and bisphenol A in Laguna Lake, Philippines. *Chemosphere* **2020**, *256*, 127122. [[CrossRef](#)]
9. Caldwell, D.J.; Mastrocco, F.; Anderson, P.D.; Lange, R.; Sumpter, J.P. Predicted-no-effect concentrations for the steroid estrogens estrone, 17 beta-estradiol, estriol, and 17 alpha-ethinylestradiol. *Environ. Toxicol. Chem.* **2012**, *31*, 1396–1406. [[CrossRef](#)]
10. Anderson, P.D.; Johnson, A.C.; Pfeiffer, D.; Caldwell, D.J.; Hannah, R.; Mastrocco, F.; Sumpter, J.P.; Williams, R.J. Endocrine disruption due to estrogens derived from humans predicted to be low in the majority of U.S. surface waters. *Environ. Toxicol. Chem.* **2012**, *31*, 1407–1415. [[CrossRef](#)]
11. Mirnasab, M.A.; Hashemi, H.; Samaei, M.R.; Azhdarpoor, A. Advanced removal of water NOM by pre-ozonation, enhanced coagulation and bio-augmented granular activated carbon. *Int. J. Environ. Sci. Technol.* **2021**, *18*, 3143–3152. [[CrossRef](#)]
12. Honorio, J.F.; Veit, M.T.; Suzaki, P.Y.R.; Coldebella, P.F.; Rigobello, E.S.; Tavares, C.R.G. Adsorption of natural hormones estrone, 17 beta-estradiol, and estriol by rice husk: Monocomponent and multicomponent kinetics and equilibrium. *Environ. Technol.* **2020**, *41*, 1075–1092. [[CrossRef](#)] [[PubMed](#)]
13. Yin, Z.H.; Liu, Y.G.; Tan, X.F.; Jiang, L.H.; Zeng, G.M.; Liu, S.B.; Tian, S.R.; Liu, S.J.; Liu, N.; Li, M.F. Adsorption of 17 beta-estradiol by a novel attapulgite/biochar nanocomposite: Characteristics and influencing factors. *Process Saf. Environ.* **2019**, *121*, 155–164. [[CrossRef](#)]
14. Jiang, L.H.; Liu, Y.G.; Zeng, G.M.; Liu, S.B.; Que, W.; Li, J.; Li, M.F.; Wen, J. Adsorption of 17 beta-estradiol by graphene oxide: Effect of heteroaggregation with inorganic nanoparticles. *Chem. Eng. J.* **2018**, *343*, 371–378. [[CrossRef](#)]
15. Xu, Z.X.; Zhang, J.; Cong, L.; Meng, L.; Song, J.M.; Zhou, J.; Qiao, X.G. Preparation and characterization of magnetic chitosan microsphere sorbent for separation and determination of environmental estrogens through SPE coupled with HPLC. *J. Sep. Sci.* **2011**, *34*, 46–52. [[CrossRef](#)] [[PubMed](#)]
16. Yang, Y.K.; Yan, W.Y.; Guo, C.X.; Zhang, J.H.; Yu, L.G.; Zhang, G.H.; Wang, X.M.; Fang, G.Z.; Sun, D.D. Magnetic molecularly imprinted electrochemical sensors: A review. *Anal. Chim. Acta* **2020**, *1106*, 1–21. [[CrossRef](#)]
17. Pan, J.M.; Chen, W.; Ma, Y.; Pan, G.Q. Molecularly imprinted polymers as receptor mimics for selective cell recognition. *Chem. Soc. Rev.* **2018**, *47*, 5574–5587. [[CrossRef](#)]
18. Yagishita, M.; Kubo, T.; Nakano, T.; Shiraiishi, F.; Tanigawa, T.; Naito, T.; Sano, T.; Nakayama, S.F.; Nakajima, D.; Otsuka, K. Efficient extraction of estrogen receptor-active compounds from environmental surface water via a receptor-mimic adsorbent, a hydrophilic PEG-based molecularly imprinted polymer. *Chemosphere* **2019**, *217*, 204–212. [[CrossRef](#)]
19. Huang, K.; Wang, X.; Zhang, H.X.; Zeng, L.S.; Zhang, X.; Wang, B.M.; Zhou, Y.K.; Jing, T. Structure-Directed Screening and Analysis of Thyroid-Disrupting Chemicals Targeting Transthyretin Based on Molecular Recognition and Chromatographic Separation. *Environ. Sci. Technol.* **2020**, *54*, 5437–5445. [[CrossRef](#)]
20. Jin, W.B.; Zhou, T.; Li, G.K. Recent advances of modern sample preparation techniques for traditional Chinese medicines. *J. Chromatogr. A* **2019**, *1606*, 460377. [[CrossRef](#)]
21. Chen, J.L.; Zhao, W.H.; Tan, L.J.; Wang, J.F.; Li, H.P.; Wang, J.T. Separation and detection of trace atrazine from seawater using dummy-template molecularly imprinted solid-phase extraction followed by high-performance liquid chromatography. *Mar. Pollut. Bull.* **2019**, *149*, 110502. [[CrossRef](#)] [[PubMed](#)]

22. Li, Z.G.; Wang, J.J.; Chen, X.; Hu, S.Y.; Gong, T.T.; Xian, Q.M. A novel molecularly imprinted polymer-solid phase extraction method coupled with high performance liquid chromatography tandem mass spectrometry for the determination of nitrosamines in water and beverage samples. *Food Chem.* **2019**, *292*, 267–274. [[CrossRef](#)] [[PubMed](#)]
23. Chen, L.G.; Zhang, X.P.; Xu, Y.; Du, X.B.; Sun, X.; Sun, L.; Wang, H.; Zhao, Q.; Yu, A.M.; Zhang, H.Q.; et al. Determination of fluoroquinolone antibiotics in environmental water samples based on magnetic molecularly imprinted polymer extraction followed by liquid chromatography-tandem mass spectrometry. *Anal. Chim. Acta* **2010**, *662*, 31–38. [[CrossRef](#)] [[PubMed](#)]
24. Wei, X.X.; Wang, Y.Z.; Chen, J.; Ni, R.; Meng, J.J.; Liu, Z.W.; Xu, F.T.; Zhou, Y.G. Ionic liquids skeleton typed magnetic core-shell molecularly imprinted polymers for the specific recognition of lysozyme. *Anal. Chim. Acta* **2019**, *1081*, 81–92. [[CrossRef](#)] [[PubMed](#)]
25. Zhang, Z.L.; Wang, H.M.; Wang, H.L.; Wu, C.C.; Li, M.L.; Li, L. Fabrication and evaluation of molecularly imprinted magnetic nanoparticles for selective recognition and magnetic separation of lysozyme in human urine. *Analyst* **2018**, *143*, 5849–5856. [[CrossRef](#)]
26. Li, X.; Ma, X.G.; Huang, R.F.; Xie, X.W.; Guo, L.H.; Zhang, M.Y. Synthesis of a molecularly imprinted polymer on mSiO<sub>2</sub>@Fe<sub>3</sub>O<sub>4</sub> for the selective adsorption of atrazine. *J. Sep. Sci.* **2018**, *41*, 2837–2845. [[CrossRef](#)]
27. Zhao, Q.Y.; Zhao, H.T.; Yang, X.; Zhang, H.; Dong, A.J.; Wang, J.; Li, B. Selective recognition and fast enrichment of anthocyanins by dummy molecularly imprinted magnetic nanoparticles. *J. Chromatogr. A* **2018**, *1572*, 9–19. [[CrossRef](#)]
28. Yu, X.L.; Liu, H.; Diao, J.X.; Sun, Y.; Wang, Y.C. Magnetic molecularly imprinted polymer nanoparticles for separating aromatic amines from azo dyes—Synthesis, characterization and application. *Sep. Purif. Technol.* **2018**, *204*, 213–219. [[CrossRef](#)]
29. Xie, X.Y.; Hu, Q.; Ke, R.F.; Zhen, X.Y.; Bu, Y.S.; Wang, S.C. Facile preparation of photonic and magnetic dual responsive protein imprinted nanomaterial for specific recognition of bovine hemoglobin. *Chem. Eng. J.* **2019**, *371*, 130–137. [[CrossRef](#)]
30. Parvaresh, V.; Hashemi, H.; Khodabakhshi, A.; Sedehi, M. Removal of dye from synthetic textile wastewater using agricultural wastes and determination of adsorption isotherm. *Desalin. Water Treat.* **2018**, *111*, 345–350. [[CrossRef](#)]
31. Zhou, X.X.; Lai, C.; Huang, D.L.; Zeng, G.M.; Chen, L.; Qin, L.; Xu, P.; Cheng, M.; Huang, C.; Zhang, C.; et al. Preparation of water-compatible molecularly imprinted thiol-functionalized activated titanium dioxide: Selective adsorption and efficient photodegradation of 2, 4-dinitrophenol in aqueous solution. *J. Hazard. Mater.* **2018**, *346*, 113–123. [[CrossRef](#)] [[PubMed](#)]
32. Azizi, A.; Bottaro, C.S. A critical review of molecularly imprinted polymers for the analysis of organic pollutants in environmental water samples. *J. Chromatogr. A* **2020**, *1614*, 460603. [[CrossRef](#)] [[PubMed](#)]
33. Adeola, A.O.; de Lange, J.; Forbes, P.B.C. Adsorption of antiretroviral drugs, efavirenz and nevirapine from aqueous solution by graphene wool: Kinetic, equilibrium, thermodynamic and computational studies. *Appl. Surf. Sci. Adv.* **2021**, *6*, 100157. [[CrossRef](#)]
34. Fang, L.; Miao, Y.X.; Wei, D.; Zhang, Y.; Zhou, Y.C. Efficient removal of norfloxacin in water using magnetic molecularly imprinted polymer. *Chemosphere* **2021**, *262*, 128032. [[CrossRef](#)] [[PubMed](#)]
35. Bi, L.; Chen, Z.; Li, L.; Kang, J.; Zhao, S.; Wang, B.; Yan, P.; Li, Y.; Zhang, X.; Shen, J. Selective adsorption and enhanced photodegradation of diclofenac in water by molecularly imprinted TiO<sub>2</sub>. *J. Hazard. Mater.* **2021**, *407*, 124759. [[CrossRef](#)]
36. Zhang, C.; Lai, C.; Zeng, G.M.; Huang, D.L.; Yang, C.P.; Wang, Y.; Zhou, Y.Y.; Cheng, M. Efficacy of carbonaceous nanocomposites for sorbing ionizable antibiotic sulfamethazine from aqueous solution. *Water Res.* **2016**, *95*, 103–112. [[CrossRef](#)]
37. Ilktac, R.; Gumus, Z.P.; Aksuner, N. Development of rapid, sensitive and selective fluorimetric method for determination of 1-naphthalene acetic acid in cucumber by using magnetite-molecularly imprinted polymer. *Spectrosc. Acta Part A-Mol. Biomol. Spectrosc.* **2019**, *218*, 62–68. [[CrossRef](#)]
38. Zhou, Z.Y.; Liu, X.T.; Zhang, M.H.; Jiao, J.; Zhang, H.W.; Du, J.; Zhang, B.; Ren, Z.Q. Preparation of highly efficient ion-imprinted polymers with Fe<sub>3</sub>O<sub>4</sub> nanoparticles as carrier for removal of Cr(VI) from aqueous solution. *Sci. Total Environ.* **2020**, *699*, 134334. [[CrossRef](#)]
39. Dil, E.A.; Doustimotlagh, A.H.; Javadian, H.; Asfaram, A.; Ghaedi, M. Nano-sized Fe<sub>3</sub>O<sub>4</sub>@SiO<sub>2</sub>-molecular imprinted polymer as a sorbent for dispersive solid-phase microextraction of melatonin in the methanolic extract of *Portulaca oleracea*, biological, and water samples. *Talanta* **2021**, *221*, 121620. [[CrossRef](#)]
40. Hsu, L.J.; Lee, L.T.; Lin, C.C. Adsorption and photocatalytic degradation of polyvinyl alcohol in aqueous solutions using P-25 TiO<sub>2</sub>. *Chem. Eng. J.* **2011**, *173*, 698–705. [[CrossRef](#)]
41. Ren, Y.M.; Yang, J.; Ma, W.Q.; Ma, J.; Feng, J.; Liu, X.L. The selective binding character of a molecular imprinted particle for Bisphenol A from water. *Water Res.* **2014**, *50*, 90–100. [[CrossRef](#)] [[PubMed](#)]
42. Nguyen, M.N.; Weidler, P.G.; Schwaiger, R.; Schafer, A.I. Interactions between carbon-based nanoparticles and steroid hormone micropollutants in water. *J. Hazard. Mater.* **2021**, *402*, 122929. [[CrossRef](#)] [[PubMed](#)]
43. Xu, H.H.; Han, Y.P.; Wang, G.Z.; Deng, P.Y.; Feng, L.L. Walnut shell biochar based sorptive remediation of estrogens polluted simulated wastewater: Characterization, adsorption mechanism and degradation by persistent free radicals. *Environ. Technol. Inno.* **2022**, *28*, 102870. [[CrossRef](#)]
44. Rana, A.G.; Hussain, M.Z.; Hammond, N.; Luca, S.V.; Fischer, R.A.; Minceva, M. Synthesis of highly active doped graphitic carbon nitride using acid-functionalized precursors for efficient adsorption and photodegradation of endocrine-disrupting compounds. *Chemistryselect* **2022**, *7*, e20220190.
45. Yasir, M.; Ngwabebhoh, F.A.; Sopik, T.; Lovecka, L.; Kimmer, D.; Sedlarik, V. The adsorptive behaviour of electrospun hydrophobic polymers for optimized uptake of estrogenic sex hormones from aqueous media: Kinetics, thermodynamics, and reusability study. *J. Chem. Technol. Biot.* **2022**, *97*, 3317–3332. [[CrossRef](#)]

46. Martins, D.S.; Estevam, B.R.; Perez, I.D.; Americo-Pinheiro, J.H.P.; Isique, W.D.; Boina, R.F. Sludge from a water treatment plant as an adsorbent of endocrine disruptors. *J. Environ. Chem. Eng.* **2022**, *10*, 108090. [[CrossRef](#)]
47. Honorio, J.F.; Veit, M.T.; Suzaki, P.Y.R.; Tavares, C.R.G.; Barbieri, J.C.Z.; Tavares, F.D.; Lied, E.B. Single and multi-component removal of natural hormones from aqueous solutions using soybean hull. *J. Environ. Chem. Eng.* **2022**, *10*, 107995. [[CrossRef](#)]
48. Deng, P.Y.; Wang, G.Z.; Li, C.K.; Dou, S.T.; Yuan, W. Removal of estrogen pollutants using biochar-pellet-supported nanoscale zero-valent iron. *Water Sci. Technol.* **2022**, *85*, 3259–3270. [[CrossRef](#)]
49. Kirec, O.; Alacabey, I.; Erol, K.; Alkan, H. Removal of 17 beta-estradiol from aqueous systems with hydrophobic microspheres. *J. Polym. Eng.* **2021**, *41*, 226–234. [[CrossRef](#)]
50. Wang, L.; Chen, G.N.; Shu, H.; Cui, X.; Luo, Z.M.; Chang, C.; Zeng, A.G.; Zhang, J.; Fu, Q. Facile covalent preparation of carbon nanotubes/amine-functionalized Fe<sub>3</sub>O<sub>4</sub> nanocomposites for selective extraction of estradiol in pharmaceutical industry wastewater. *J. Chromatogr. A* **2021**, *1638*, 461889. [[CrossRef](#)]
51. Li, Y.X.; Hu, B.Y.; Gao, S.Y.; Tong, X.; Jiang, L.S.; Chen, X.C.; An, S.Y.; Zhang, F.S. Comparison of 17 beta-estradiol adsorption on soil organic components and soil remediation agent-biochar. *Environ. Pollut.* **2020**, *263*, 114572. [[CrossRef](#)] [[PubMed](#)]